Available online at www.sciencedirect.com

SciVerse ScienceDirect

Procedia CIRP 8 (2013) 570 – 575

www.elsevier.com/locate/procedia

14th CIRP Conference on Modeling of Machining Operations (CIRP CMMO)

Optimization of Serrated End Mills for Reduced Cutting Energy and Higher Stability

R. Koca and E. Budak*

[a]*Manufacturing Research Laboratory,Sabanci University, Tuzla, Istanbul-34956, Turkey*

* Corresponding author. Tel.:+ 90-216-483 9519; fax: +90-216-483-9550; *E-mail address*: ebudak@sabanciuniv.edu

Abstract

Although serrated end mills are commonly used in machining industry, the literature on these tools is limited to predictive methods while no work has been reported on selection, design or optimization of serration forms. In this paper, mechanics and dynamics of these tools are modeled and experimentally verified. Linear edge-force model is adopted for force modeling whereas first order semi-discretization method including multiple delays with time-averaged coefficient matrices is used for stability analysis. Frequently used serration waveforms, i.e. sinusoidal, circular and trapezoidal are modeled parametrically and optimized for reduced milling forces using the Brute Force Search and the Differential Evolution Method. The superior performance of the optimized serrated end mills is demonstrated in terms of reduced milling forces and increased stability.

Selection and peer-review under responsibility of The International Scientific Committee of the "14th CIRP Conference on Modeling of Machining Operations" in the person of the Conference Chair Prof. Luca Settineri

Keywords: Serrated End Mills; Mechanics; Dynamics; Chatter Stability, Optimization

1. Introduction

Reduced milling forces, increased chatter stability and superior chip breaking make serrated end mills favorable in machining operations, especially in roughing. Although serrated end mills are often used in industry, the literature on these tools is limited. Tlusty et al. [1] investigated the chatter stability of serrated end mills using time-domain solutions and a simplified approach. They observed that serrated end mills lower total tool-workpiece contact length which decreases the effective axial depth of cut increasing the absolute stability limit considerably. They also showed added stability pockets in the stability diagram. Campomanes et al. [2] formulated mechanics and dynamics models for serrated end mills having sinusoidal serration waveform using a kinematics of milling model for the calculation of the local chip thickness. An analytical stability prediction method based on [3] is presented for serrated end mills. Wang and Yang [4] presented a force model for cylindrical end mills having sinusoidal serration form. They observed that with appropriate feed per tooth values, at an axial position only one cutting tooth removes the material. Because of this, the chip thickness for that tooth becomes equal to the total feed per revolution. Merdol and Altintas [5] proposed force and time-domain stability models for cylindrical and tapered end mills with serrated cutting teeth. Serration profile is modeled using cubic splines which allow the inclusion of different serration forms into the models. Dombovari et al. [6] proposed a stability model for serrated end mills. Unlike previous works, they solved the stability of milling with serrated end mills by using the Semi-Discretization Method. Yusoff and Sims [7] optimized variable pitch and helix angles for a given milling system by using the Differential Evolution (DE) method presented by Storn and Price [8].

In this study, common serration wave forms, i.e. sinusoidal, circular and trapezoidal are modeled parametrically. Milling forces are modeled using the linear edge force model where the cutting force coefficients are obtained by orthogonal-to-oblique

Selection and peer-review under responsibility of The International Scientific Committee of the "14th CIRP Conference on Modeling of Machining Operations" in the person of the Conference Chair Prof. Luca Settineri

doi:10.1016/j.procir.2013.06.152

transformation [9]. Stability of milling with serrated end mills is investigated with the first order Semi-Discretization Method including multiple delays and time-averaged coefficient matrices. In addition, serration waveform parameters are optimized using Brute Force Search (BF) and DE. Predicted parameters are used for comparison with standard serrated end mills available in the market in terms of chatter stability and milling forces.

2. Serrated End Mill Geometry

It is essential to understand the details of the serrated cutting edge geometry in order to model mechanics and dynamics of milling for these tools. The cutting teeth have ground waves on their flank faces. The waves on consecutive cutting teeth have a phase shift in tool axis direction. Because of the ground waves and the phase shift, at a certain z level, consecutive cutting teeth have different radii. In Fig 1, a) cross-section of a serrated end mill at a certain z level, b) surface tangent, normal vectors and K angle is given. In Fig 2, frequently used serration forms and their defining parameters can be seen.

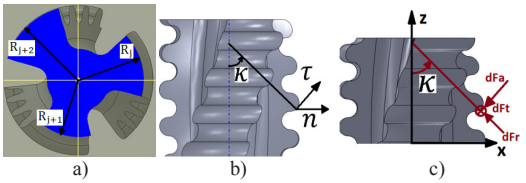

a) b) c)

Fig. 1. (a) Serrated end mill cross-section; (b) Surface tangent vector $\boldsymbol{\tau}$, surface normal vector $\boldsymbol{n}$ and K (axial immersion) angle ; (c) differential milling forces and their directions

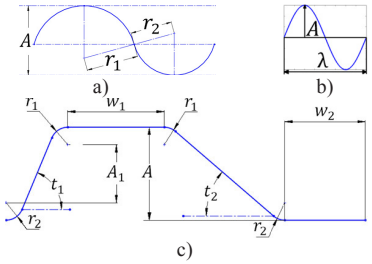

Fig. 2. Serration waveforms (a) circular; (b) sinusoidal; (c) trapezoidal

Rake and oblique angles vary along serrated cutting edges. In Fig 3 a), three sections of a serrated cutting edge, which has a rectangular serration form, are marked. In Fig 3 b) and c) helix (global oblique) and rake angles of the cutting tooth are illustrated.

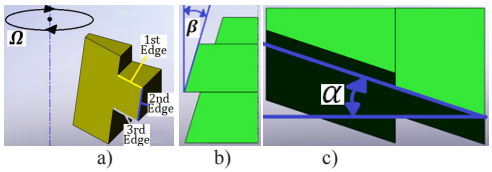

a) b) c)

Fig. 3. (a) Fraction of a serrated edge; (b) global oblique angle β (right view); (c) global rake angle α (top view)

In Fig 4, the first edge is illustrated. From cutting mechanics point of view, the local rake angle is the negative of the helix angle. The local oblique angle on this edge is equal to the rake angle of the end mill.

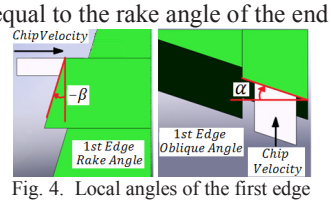

Fig. 4. Local angles of the first edge

In Fig 5 (a), local angles of the 2nd edge are shown. On this edge, the local rake and oblique (helix) angles are the same as the ones for the end mill.

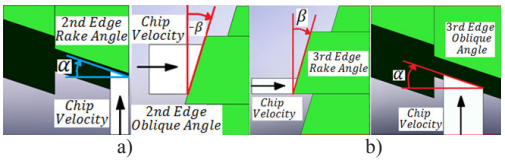

a) b)

Fig. 5. (a)Local angles of the second edge and the third (b)

In Fig 5 b), the 3rd edge is given. On this edge, the local rake angle is equal to the tool's helix angle while the oblique angle is equal to its rake angle. As a summary, upper part of the serration has lower rake angles while lower part of the serration has higher ones. This generalization is valid for all types of serration waves. It is a known fact that increasing rake angle affects the shearing mechanism positively. When selecting or designing serrated end mills, one can exploit this. However, in order to use this as an advantage, cutting edge strength also needs to be taken into account since as the rake angle increases the cutting edge strength decreases. It should also be noted that for most serration types such as sinusoidal, circular and trapezoidal, resulting change in the rake and oblique angles is not as drastic as in the case of rectangular or square wave types. However, it should be noted that serrated end mills are employed with lower feed per tooth which decreases the immersed part of the cutting edges, thus the local angle variations. This situation can be controlled by choosing the phase shift direction between the serration waves of the consecutive teeth. The phase difference between the j^{th} and the first teeth for serrated end mills is $\left(\frac{\lambda}{Nt}\right) * (j-1)$, where λ, Nt and j represent wavelength of the serration, number of teeth and tooth number, respectively.

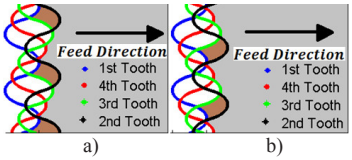

a) b)

Fig. 6. (a) Lower and (b) higher rake sections

Users can distinguish these two types by looking at the

directions of the flute and the serration helixes. If they have the same direction, e.g. both right hand, then the sections with lower rake angles will remove material. If their directions are opposite, then the sections with higher rake angles remove material.

3. Force Model

In Fig. 1 (c), differential milling forces are illustrated. Because of the serrations, the directions of the differential milling forces vary along the cutting edges. Milling tool is divided into small disc elements along the tool axis for force calculations. The differential forces are calculated for every tooth at every axial disc element and immersion angle within one tool revolution. The axial, radial and tangential differential forces acting on the j^{th} tooth at axial level z for the immersion angle $\emptyset$ are given in (1) where db represents the chip width.

$$\begin{aligned} dFa_j(\emptyset_j, z) &= g(\emptyset_j)\left[K_{ae} + K_{ac}\, h_j(\emptyset_j, z)\right]db \\ dFr_j(\emptyset_j, z) &= g(\emptyset_j)\left[K_{re} + K_{rc}\, h_j(\emptyset_j, z)\right]db \\ dFt_j(\emptyset_j, z) &= g(\emptyset_j)\left[K_{te} + K_{tc}\, h_j(\emptyset_j, z)\right]db \\ db &= dz \Big/ \sin(\kappa(z, j)) \end{aligned} \quad (1)$$

Kae, Kre, Kte; Kac, Krc and Ktc are the edge and cutting force coefficients, respectively. Chip thickness is calculated as in (2), where $h_j(\emptyset, z)$, $R_j(z)$, ft are the chip thickness for the j^{th} tooth at axial level z for the immersion angle $\emptyset$, local radius for j^{th} tooth and feed per tooth, respectively.

$$h_j(\emptyset, z) = \max(0, h_j v), \qquad m = \begin{Bmatrix} Nt & \leftarrow \text{if } j - k = 0 \\ & \text{else} \\ \mod((j-k), Nt) & \end{Bmatrix} \quad (2)$$

$$h_j v(\emptyset, z) = \min \begin{bmatrix} R_j(z) - R_m(z) + k * ft \\ * \sin(\emptyset_j(z)) \end{bmatrix}, \quad k = 1, 2, \dots, Nt$$

In Fig 7, a regular and a serrated end mill are compared in terms of local chip thickness for the same given milling conditions. Radial immersion is 6mm, ft=0.05mm/tooth, axial depth of cut is 8mm, R=6mm, Nt=4. The serrated end mill has the circular serration wave form with the following geometrical parameters: $r_1 = 0.5\text{mm}, r_2 = 0.5\text{mm}, A = 0.6\, mm.$ Milling operation is in down-milling mode. At a certain axial level, only one cutting tooth removes material. Since the other ones do not, the tooth in-cut removes the whole feed per revolution at that axial level. This causes the local chip thicknesses to increase up to $ft * Nt$ as can be seen from the figure, if the radial immersion is higher or equal to half immersion. As the chip thickness increases, the cutting force coefficients decrease.

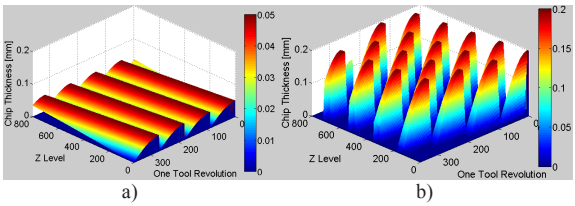

a) b)

Fig. 7. (a) Chip load for regular tool, (b) chip load for serrated tool.

Most importantly, total contact between the workpiece and the tool decreases drastically, and thus so do the edge forces. The forces acting on the tool in X,Y,Z directions are calculated, as given in (1), (3) and (4), where a is the axial depth of cut.

$$F_{x,y,z}(\emptyset) = \sum_{z=0}^{z=a} \sum_{j=1}^{j=Nt} dF_{xj,yj,zj}(\emptyset_j, z) \quad (4)$$

Milling tests were carried out with serrated end mills on a DMG 5-axis machining center. Data is collected with NI USB DAQ and LabView software. One full revolution of the end mill is represented with 180 data points, thus the sampling frequency is adjusted according to spindle speed. An Al7075 block mounted on the dynamometer, is machined. A serrated tool having 12mm diameter with 4 cutting teeth, 30° helix, and trapezoidal serration waveform is used in the tests. The serration parameters are; $r_1 = r_2 = 0.2$mm , $W_1 = 0.3$ mm , $W_2 = 0.2$mm, $t_1 = t_2 = 45°$, A=0.5mm. Process is down-milling. In Fig 8, measured and predicted forces for one tool revolution are given. Experimental results and force model are in a good agreement.

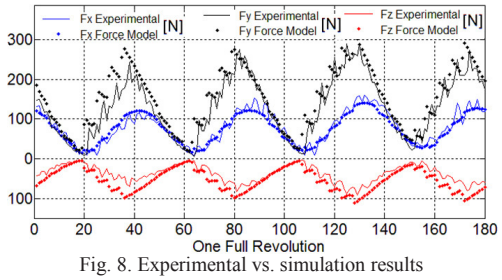

Fig. 8. Experimental vs. simulation results

4. Optimization of Serration Wave Parameters for Lower Forces

In this section, waveform parameters of the serration waves are optimized in order to minimize milling forces. The optimization process will be handled by using two methods, namely BF and DE. In BF, every possible combination is searched in order to determine the optimal parameters. It can be very time consuming, however it is a good practice to analyze the objective function behaviour over a big search space.

$$\begin{aligned} \mathbf{dF_{xj}}(\emptyset_j, z) &= -dF_{rj}\sin(\kappa)\sin(\emptyset_j) - dF_{aj}\cos(\kappa)\sin(\emptyset_j) - dF_{tj}\cos(\emptyset_j) \\ \mathbf{dF_{yj}}(\emptyset_j, z) &= -dF_{rj}\sin(\kappa)\cos(\emptyset_j) - dF_{aj}\cos(\kappa)\cos(\emptyset_j) + dF_{tj}\sin(\emptyset_j) \quad , \quad \mathbf{dF_{zj}}(\emptyset_j, z) = dF_{rj}\cos(\kappa) - dF_{aj}\sin(\kappa) \end{aligned} \quad (3)$$

Evolutionary algorithms such as DE and Genetic Algorithm (GA), on the other hand, do not search all the parameter possibilities in order to find the optimal set, thus they are faster. Objective function is chosen as the maximum milling force in X-Y plane occurring in one tool revolution. The parameters of DE are as follows [7]: Scaling Factor=0.9, Cross-over Rate=0.9, Number of Generations=250. In order to optimize the waveform parameters, some parameters of the end mill are fixed, R=6mm, Nt=4, β=30°. Axial depth of cut is fixed as 16mm as well. In this paper, DE source code by Markus Buehren [12] was adopted.

4.1. Optimization of Sinusoidal Serration Parameters

The number of parameters to be optimized is D=2 with Population size of Np=10*D=20. Parameters for Differential Evolution are adopted from the literature [7]. Search space is restricted for geometrical parameters of the sinusoidal serration form as: $A = [0 - 2](\mathrm{mm})$, $\lambda = [0 - 10](\mathrm{mm})$. DE results are given in Table 1. Both algorithms found the same optimal parameter sets. As can be interpreted from Fig 9 that wavelength of the serration wave form has a strong effect on FxyMax. However as can be seen from Fig 9, some parameter sets have similar performance. Thus, we can say that the serration waveform optimization problem is multimodal. It is seen that for higher ft, the reduction in the milling forces is not drastic as it is for lower ft. As ft increases, a bigger portion of the serrated edge immerses in the material. Thus, the total contact between the tool and the workpiece does not decrease as much as it does with lower ft. This explains the difference between 0.05mm/tooth and 0.2 mm/tooth cases.

Table 1. Optimal sinusoidal serration parameters

b = 3mm Quarter Immersion, ft = 0.05mm/tooth		
A [mm] = 0.2	λ [mm] = 2.8	FxyMAX = 382N
Regular End Mill		FxyMAX = 647N
b = 3mm Quarter Immersion, ft=0.2mm/tooth		
A [mm] = 0.2	λ [mm] = 2.8	FxyMAX = 1174N
Regular End Mill		FxyMAX = 1274N
b = 12mm Full Immersion, ft = 0.05mm/tooth		
A [mm] = 0.2	λ [mm] = 2.8	FxyMAX = 964N
Regular End Mill		FxyMAX = 1493N
b = 12mm Full Immersion, ft=0.2mm/tooth		
A [mm] = 0.3	λ [mm] = 5.8	FxyMAX = 3193N
Regular End Mill		FxyMAX = 3446N

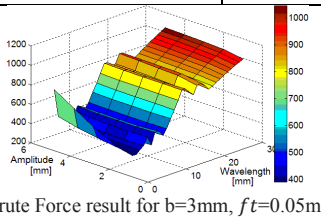

Fig. 9. Brute Force result for b=3mm, ft=0.05mm/tooth

Radial immersion affects the maximum uncut chip thickness for a given milling process. For half or higher immersions, it becomes equal to ft. However, for serrated end mills, as shown in Fig 7, maximum chip thickness can increase up to $Nt * ft$. Thus, as the maximum uncut chip thickness increases, bigger portion of the serrated edge immerses in the material. This is valid for all types of serration profiles.

4.2. Optimization of Circular Serration Parameters

For circular serration wave, there are three defining parameters, r_1, r_2, A as illustrated in Fig 2. Thus population size is increased to 10*D=30. A geometrical constraint is introduced for ensuring the arcs remain tangent to each other.

$$A \leq r_1 + r_2 \quad (5)$$

Upper and lower bounds are given in the same fashion it is done for sinusoidal serration. The constraint is included into the optimization problem with an approach called, "Brick Wall Penalty". This situation is handled inside the objective function. If a member of the current generation is violating constraint (5), the value of the objective function is not calculated; instead a very high value (e.g. 1e6) is assigned to it. This way it is ensured that the violating member does not survive to the next generation. Upper and lower bounds for the parameters are as follows: $r_1 = [0.1 - 3](\mathrm{mm})$, $r_2 = [0.1 - 3](\mathrm{mm})$, $A = [0.1 - 3](\mathrm{mm})$

Table 2: Optimal circular serration parameters

b = 3mm Quarter Immersion ft = 0.05mm/tooth			
r_1[mm]=0.5	r_2[mm]=0.5	A[mm]=0.6	FxyMAX= 376N
Regular End Mill			FxyMAX=647N
b = 3mm Quarter Immersion ft=0.2mm/tooth			
r_1[mm]=1.8	r_2[mm]=0.1	A[mm]=0.6	FxyMAX=1146N
Regular End Mill			FxyMAX=1274N
b = 12mm Full Immersion ft = 0.05mm/tooth			
r_1[mm]=1.8	r_2[mm]=2.1	A[mm]=1.3	FxyMAX=915N
Regular End Mill			FxyMAX=1493N
b = 12mm Full Immersion ft=0.2mm/tooth			
r_1[mm]=2.8	r_2[mm]=0.8	A[mm]=0.7	FxyMAX=3165N
Regular End Mill			FxyMAX=3446N

4.3 Optimization of Trapezoidal Serration Parameters

Optimization of trapezoidal serration wave form needs extra attention since the number of parameters is now increased to seven. In order to simplify the optimization process, r_1 and r_2 are kept equal and constant as 0.2mm. t_1 and t_2 are kept equal to each other at 15°, 30°, 45°, 60°, 75°. The upper and lower bounds for the parameters to be optimized are: $w_1 = [0 - 6](mm)$, $w_2 = [0 - 6](mm)$, $A = [0 - 3](mm)$. The optimal parameters are given in Table 3. The optimal parameters occurred at t_1=t_2=45°.

Table 3: Optimal trapezoidal serration parameters

b = 3mm Quarter Immersion, ft = 0.05mm/tooth			
w_1[mm]=0.3	w_2[mm]=0.2	A[mm]=0.5	FxyMAX=376 N
Regular End Mill			FxyMAX=647 N
b = 3mm Quarter Immersion, ft=0.2mm/tooth			
w_1[mm]=0.5	w_2[mm]=0	A[mm]=0.5	FxyMAX=1178N
Regular End Mill			FxyMAX=1274N
b = 12mm Full Immersion, ft = 0.05mm/tooth			
w_1[mm]=2.1	w_2[mm]=5.5	A[mm]=0.5	FxyMAX=900N
Regular End Mill			FxyMAX=1493N
b = 12mm Full Immersion, ft=0.2mm/tooth			
w_1[mm]=4.3	w_2[mm]=3.5	A[mm]=0.5	FxyMAX=3203N
Regular End Mill			FxyMAX=3446N

Table 4: Comparison of optimal vs. available serration forms from the market

Serrated Tool 1 r_1=0.78mm r_2=0.58mm A=0.25mm	b = 3mm ft=0.05 mm/tooth	b =12mm ft =0.05 mm/tooth
	FxyMAX =427N Optimum =376N	FxyMAX =1098N Optimum =900N
Serrated Tool 2 r_1=1.49mm r_2=0.975mm A=0.21mm	b = 3mm ft=0.05 mm/tooth	b =12mm ft =0.05 mm/tooth
	FxyMAX= 419N Optimum =376N	FxyMAX =1112N Optimum=900N
Serrated Tool 3 r_1=1.44mm r_2=1.035mm A=0.72mm	b = 3mm ft=0.05 mm/tooth	b =12mm ft =0.05 mm/tooth
	FxyMAX = 412N Optimum = 376N	FxyMAX = 972N Optimum=900N

Although heuristic methods do not guarantee global optimum, in this case it is verified with the BF which provided the same results. If the results for different serration types are compared, it is seen that every geometry converges to nearly the same objective function value, FxyMAX. Thus, regardless of the serration type, the same amount of performance increase can be achieved if the parameters are optimized. Three different circular serration forms available in the market are compared with the optimal forms in terms of milling forces. According to the Table 4 at least %10 improvement in terms of cutting forces is achieved with optimized serrated end mills.

5. Chatter Stability

In this section, the optimal serration parameters are compared to the standard ones from the market and to each other in terms of chatter stability. Chatter stability of serrated end mills is solved using the First Order Semi-Discretization method including multiple time delays [10] and time-averaged coefficient matrices [11].

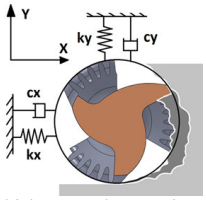

Fig. 10. Dynamic chip thickness and two orthogonal DOF

The milling stability is formulated with two orthogonal DOF as shown in Fig 10. In order to compare the serration wave parameters in terms of chatter stability, the modal parameters given in Table 5 are used.

Table 5. Modal parameters of the example system.

ω_{nx} (rad/ sec)	m_x (kg)	ζ_x	ω_{ny} (rad/ sec)	m_y (kg)	ζ_y
693*2π	0.8409	%2.503	689*2 π	0.9372	%2.947

In Fig 11 and 12, three tools are compared in terms of chatter stability for the system whose modal parameters are given in Table 5 (quarter immersion, f_t=0.05mm/tooth, R=6mm, β=30°, Nt=4). Workpiece material Al7075 is machined in down-milling mode. The serration parameters of the tools are as follows:
r_1 = 0.5mm, r_2 = 0.5mm, A = 0.6mm Optimal
r_1 = 0.78mm,r_2 = 0.58mm,A = 0.25mm Standard

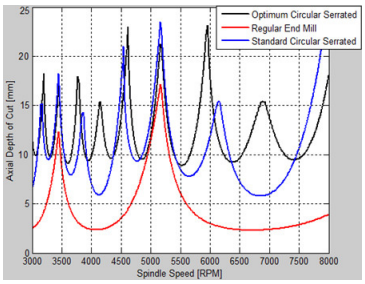

Fig. 11. Stability comparisons, 3000-8000 RPM

In Fig 11 and 12, the optimal circular serrated end mill shows a superior performance over the standard serrated end mill from the market.

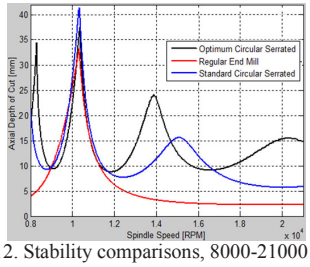

Fig. 12. Stability comparisons, 8000-21000 RPM

If serrated end mills are optimized and employed properly, absolute stability limit can be increased significantly. Added lobes occur between main lobes. This is an indication of transition of the cutting tool from a four teethed end mill to a one toothed end mill in stability point of view. In order to explain added lobes, the chip thickness distribution is illustrated for the given milling scenario. In Fig 13 resulting chip thickness and delays of the system are illustrated where $\tau_j(z)$ and T represent the delay for the j^{th} tooth at axial level z and spindle period respectively. Serrated cutting teeth remove material only at certain axial levels(Fig 13). Thus, majority of the delays in the system become one spindle period instead of tooth passing period. That is

the reason behind the added lobes in the stability diagram when using serrated end mills. There occur stability pockets at higher spindle speeds as well. A simple equation, which shows the locations of the stability pockets, is given:

$$n = \frac{60 * f_c}{k * N_t} \quad [RPM] \tag{6}$$

where n, f_c, k represent spindle speed, chatter frequency in Hz, number of the stability pocket, respectively. In Fig 11 and 12 it can be seen that for regular 4 teethed end mill stability pockets occurred according to the equation (6). However for optimized serrated end mills the added lobes are seen because the number of teeth tends to behave like 1 in stability point of view as in Fig 13. In Fig 14-15 a stability analysis is done with the same parameters given for the previous example but with an increased ft of 0.15mm/tooth. Optimized serrated end mills still show better performance than the standard serrated ones.

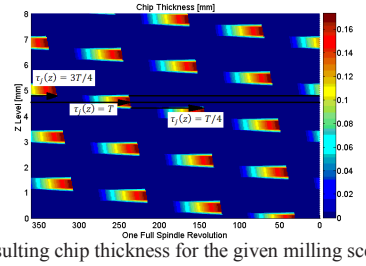

Fig. 13 Resulting chip thickness for the given milling scenario with optimal circular serrated end mill (8 mm axial doc)

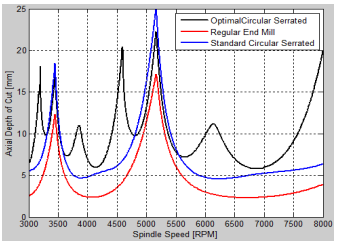

Fig. 14. Stability comparisons, 3000-8000 RPM

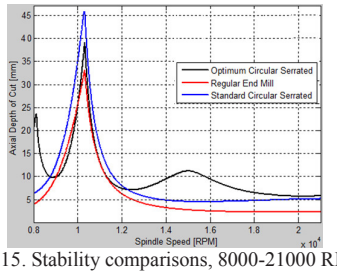

Fig. 15. Stability comparisons, 8000-21000 RPM

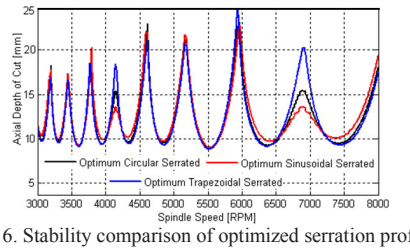

Fig. 16. Stability comparison of optimized serration profiles

However, as ft increases, one toothed behavior decreases, and thus added lobes start to diminish. In Fig 16, three different but optimized serrated forms are compared for the same given milling scenario with 0.05mm/tooth ft. It is shown that if the parameters are optimized, the same amount of stability gain can be achieved regardless of the wave type.

6. Conclusion

In this paper, geometry, mechanics and dynamics of serrated end mills are investigated. Milling forces are modeled and verified experimentally. The effects of both serration and phase shift on the varying local rake and oblique angles are discussed. Frequently used serration waveforms are optimized for lower milling forces. The effect of serration on dynamics of milling is explained. It is shown that the optimized serrated end mills achieve superior performance over standard serrated end mills in terms of both milling forces and chatter stability. The same amount of performance increase is achieved with three different types of serration waves in both resulting forces and stability.

Acknowledgements

The support of P&WC for this research is appreciated. Authors also would like to thank Mr. Çağlar Yavaş from Karcan Cutting Tools, for providing custom made serrated end mills for the verification tests.

References

[1] Tlusty, J., Ismail, F., Zaton, W., 1983, Use of special milling cutters against chatter, Technical Report, NAMRC 11, SME, University of Wisconsin , 408-415

[2] Campomanes, M., L., 2002, Kinematics and dynamics of milling with roughing end mills, Metal Cutting and High Speed Machining, Kluwer Academic/Plenum Publishers

[3] Budak, E., Altintas, E., 1998, Analytical prediction of chatter stability in milling-Part1: General formulation, Journal of Dynamic Systems, Meas. and Control 120, 22-30

[4] Wang, J., J.,J., Yang, C.S., 2003, Angle and frequency domain force models for a roughing end mill with a sinusoidal edge profile., Int. Jour. of Mach. Tools&Manuf.,43, 1509-1520

[5] Merdol, S., D., Altintas, Y., 2004, Mechanics and dynamics of serrated cylindrical and tapered end mills, Jour. of Manuf. Sci. and Eng. 126, 317-327

[6] Dombovari, Z., Altintas, Y., Stepan, G., 2010, The effect of serration on mechanics and stability of milling cutters, Int. Journ. of Mach. Tools&Manuf., 50, 511-520

[7] Yusoff, A.R., Sims, N.D., 2011, Optimization of variable helix tool geometry for regenerative chatter mitigation, Int. Journ. of Mach. Tools&Manuf., 51, 133-141

[8] Storn, R., Price, K., 1995, Differential Evolution: A simple and efficient adaptive scheme for global optimization over continuous spaces, Technical Report, Berkeley

[9] Budak, E., Altintas, Y., Armarego, E., J., 1996, Prediction of milling force coefficients from orthogonal cutting data, ASME J. Eng. Ind. 118, 216-224

[10] Insperger, T., Stepan, G., 2011, Semi-Discretization for Time-Delay Systems Stability and Engineering Applications, Applied Mathematical Sciences,17

[11] Sims, N.D., Mann, B., Huyanan, S., 2008, Analytical prediction of chatter stability for variable pitch and variable helix milling tools, Journ. of Sound and Vib., 317, 664-686

[12] B. Markus, 2008, Differential Evolution